Korean J. Chem. Eng., 34(10), 2738-2747 (2017)
DOI: 10.1007/s11814-017-0160-8

pISSN: 0256-1115
eISSN: 1975-7220

Synthesis of pillar and microsphere-like magnesium oxide particles and their fluoride adsorption performance in aqueous solutions

Sang Goo Lee, Jong-Wook Ha†, Eun-Ho Sohn, In Jun Park, and Soo-Bok Lee

Advanced Materials Division, Korea Research Institute of Chemical Technology,
Gajeong-ro 141, Yuseong-gu, Daejeon 34114, Korea
(*Received 23 January 2017 • accepted 7 June 2017*)

Abstract−We synthesized pillar and microsphere-like MgO particles and their fluoride removal performance. Samples of MgO were synthesized by calcination of precursors derived from $MgCO_3 \cdot 3H_2O$ and characterized using field emission scanning electron microscopy, X-ray diffraction, and N_2 adsorption-desorption isotherms. The fluoride removal performance of the MgO samples was investigated in terms of adsorption kinetics and adsorption equilibrium. The effects of pH and the presence of other anions on the fluoride adsorption were also considered. The adsorption capacities of pillar and microsphere-like MgO particles were 151.51 and 166.66 mg/g, respectively. The pH of the aqueous solutions did not significantly affect the fluoride adsorption at pH 9 or lower. Except for phosphate, the effect of co-existing anions on fluoride adsorption was not considerable. Fluoride removal occurred through the substitution of hydroxyl groups on the surface of MgO with fluorides.

Keywords: Magnesium Oxide, Synthesis, Fluoride Removal, Adsorbent, Particle Morphology

INTRODUCTION

The types of mineral ions and their concentration in groundwater are important factors that determine the water quality. Fluoride ions, especially, in groundwater have attracted considerable attention because they are closely related to human health. Excessive fluoride intake causes serious dental and skeletal fluorosis and also damages the DNA structure [1-3]. According to the World Health Organization (WHO) guidelines, the concentration of fluoride in drinking water must be less than 1.5 mg/L [4]. Treatment of fluoride ions in industrial wastewater is also an important and long-lasting issue. Technologies such as chemical precipitation, adsorption, membrane processes, and ion exchange have been developed for the removal of fluorides from aqueous solutions [5]. Of these, adsorption has been an economical and effective method [6,7]. Various adsorbents have been studied for fluoride removal [8-15]. Among the available adsorbents, metal oxides with high surface areas have attracted significant attention in water treatment [16-21]. In particular, magnesium oxide is a nontoxic and environmentally friendly material that has shown excellent performance for fluoride removal from contaminated aqueous solutions as well as other pollutants [22-30].

Recently, studies on the preparation of MgO with large surface areas and excellent adsorption performance have been conducted. Qu et al. reported flower-like MgO microspheres with a specific surface area of 43.6 m^2/g, which were prepared by calcination of flower-like hydrated magnesium carbonate hydroxide formed by the hydrothermal treatment of a mixture of $MgCl_2$ and Na_2CO_3 [31]. According to Zhou et al., hierarchical hydromagnesite microspheres could be prepared by the hydrothermal treatment of a mixture of $MgCl_2$ and Na_2CO_3 in the presence of sodium poly(4-styrenesulfonate). After calcination, the specific surface area of the obtained mesoporous MgO microspheres was 72.1 m^2/g [32]. Li et al. reported the synthesis of porous hollow MgO microspheres with a specific surface area of 130.0 m^2/g, which were prepared by calcination of the microsphere precursor formed by hydrothermal treatment of a mixture of $MgCl_2$ and urea in a solution of water and ethylene glycol [27]. Purwajanti et al. reported the synthesis of MgO microspheres with a specific surface area in the range of 16-194 m^2/g by adjusting calcination temperatures [33].

Previous studies focused on the specific surface area and adsorption characteristics of microsphere-like MgO particles. In contrast, studies on the adsorption performance of pillar-like MgO have been relatively rare. Furthermore, there is no report comparing the fluoride adsorption performances of pillar and microsphere-like MgO. Herein, we report the synthesis of MgO by calcination of pillar and microsphere-like precursors and their fluoride removal performance. Both MgO samples and their precursors were characterized by field emission scanning electron microscopy (FE-SEM), X-ray diffraction (XRD), and N_2 adsorption-desorption isotherms. The fluoride removal performance of samples was also investigated in terms of adsorption kinetics and equilibria, and various experimental conditions such as pH of aqueous solutions and the presence of other anions.

EXPERIMENTAL SECTION

1. Synthesis

Magnesium chloride hexahydrate ($MgCl_2 \cdot 6H_2O$, 98%) and sodium carbonate (Na_2CO_3, 99%) were both analytical grade and

†To whom correspondence should be addressed.
E-mail: jongwook@krict.re.kr
Copyright by The Korean Institute of Chemical Engineers.

used without further purification. In a typical synthesis of pillar-like precursors, $MgCO_3 \cdot 3H_2O$, a 200 mL aqueous solution of 0.63 M Na_2CO_3 was added dropwise into 600 mL of 0.21 M $MgCl_2 \cdot 6H_2O$ with vigorous magnetic stirring at 30 °C for 1 h. The mixed solution was then kept in an isothermal state for 24 h without stirring. After reaction, the precipitate was washed with deionized water and dried under vacuum at 60 °C for 48 h. In a typical synthesis of microsphere-like precursors, $Mg_5(CO_3)_4(OH)_2 \cdot 4H_2O$, the mixed solution described above was transferred into a Teflon-lined stainless steel autoclave with a capacity of 1,000 mL. The autoclave was sealed and heated to 80 °C using a convection oven and kept in an isothermal state for 24 h. The precipitate was washed with deionized water and finally dried under vacuum pressure at 60 °C for 24 h. To obtain MgO, the as-synthesized precursors were calcined in an electrical furnace at 500 °C for 6 h.

2. Characterization

FE-SEM images were taken with a JEOL JSM-6700F instrument operating at 10 kV. Powder XRD patterns were obtained by using a Rigaku D-MAX-2200V X-Ray diffractometer and Cu Kα radiation (wavelength λ=1.5418 Å) at room temperature. X-ray photoelectron spectroscopy (XPS) was performed using a KRATOS AXIS NOVA with an Al-Kα X-ray source at 15 keV operating at 150 W. Transmission electron microscopy (TEM) images were obtained with a JEOL 1200 EX II operating at 80 kV or a Phillips 420 operating at 120 kV. Energy dispersive spectrometer (EDS) measurements were obtained by using a Bruker Quantax 200 with a Si drift detector. The specific surface areas of the samples were measured by Brunauer-Emmett-Teller (BET) method by recording nitrogen adsorption/desorption isotherms at 77 K (Couter Omnisorp 100CX). The pore size distributions were calculated by Barret-Joyner-Halenda (BJH) method.

3. Fluoride Adsorption Experiments

Batch adsorption experiments were conducted to examine the performance of MgO samples as fluoride adsorbents. All experiments were in 100 mL polypropylene flasks containing 50 mL of fluoride solution at 25 °C and in triplicate. After adding 0.05 g of as-synthesized precursors or MgO particles to the fluoride solution, the mixture was stirred magnetically for 3 h. After the adsorption experiments, the adsorbent was separated using a PVDF filter and the concentration of fluoride ions in the filtrate was measured using a ion selective meter (Star A214, Thermo Scientific Orion) with the fluoride ion selective electrode (9609BNWP, Thermo Scientific Orion). Sodium fluoride (NaF, 99%, Sigma-Aldrich Korea) aqueous solution with fluoride concentration of 100 mg/L was used in the adsorption kinetics studies. The adsorption equilibria were investigated by using NaF aqueous solutions having various fluoride concentrations (5, 10, 20, 30, 50, 100, 200, 300, 500, 700, and 1,000 mg/L).

The effect of pH on fluoride adsorption was studied after adjusting the pH of the fluoride solutions with an aqueous solution of HCl or NaOH. The effects of other anions, such as carbonate, bicarbonate, and phosphate, on adsorption were examined at neutral pH condition. The concentrations of anion in the fluoride solutions were adjusted to 0.1 mM, 1 mM and 10 mM, respectively. In these experiments, the initial fluoride concentration was fixed to 10 mg/L.

The fluoride adsorption capacity was calculated by using the following equation:

$$q_e = \frac{(C_0 - C_e)V}{m} \quad (1)$$

where C_0 and C_e represent the initial and equilibrium fluoride con-

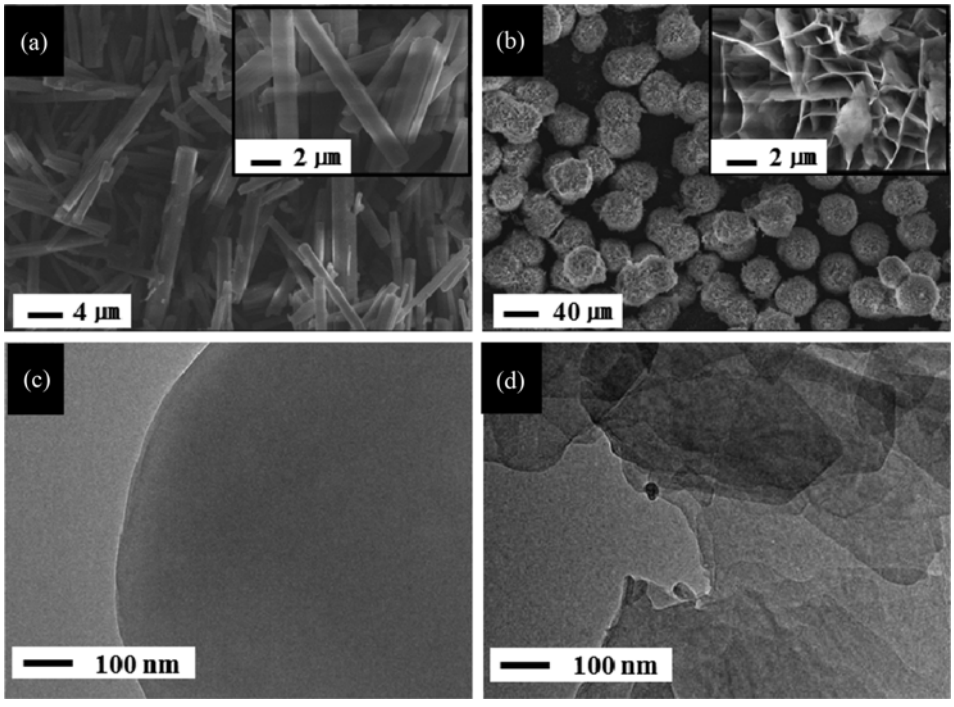

Fig. 1. SEM and TEM images of precursors produced at 30 °C (a), (c) and 80 °C (b), (d).

centrations (mg/L), respectively, V is the volume of the fluoride solution (L), and m is the amount of adsorbent (g). The removal percentage of fluoride was calculated from the following equation:

$$\% \text{ removal} = \left(1 - \frac{C_e}{C_0}\right) \times 100 \quad (2)$$

The used adsorbents were washed with deionized water and dried under vacuum pressure at 60 °C for 24 h. Then adsorbents were calcined in an electrical furnace at 500 °C for 3 h for regeneration and recycling experiments.

RESULTS AND DISCUSSION

1. Synthesis and Characterization of MgO Adsorbents

To investigate the effect of adsorbent morphology on the fluoride removal efficiency from aqueous solutions, two different types of MgO precursor were prepared from hydrothermal process. Fig. 1 shows SEM and TEM images of precursors produced at 30 and 80 °C. At the lower reaction temperature, pillar-like precursors, which were about 20 μm in length and 2 μm in diameter, were obtained as can be observed in Fig. 1(a). According to TEM image shown in Fig. 1(c), their surfaces were smooth and non-porous. In contrast, the microsphere-like precursors consisted of assemblies of flakes were produced at 80 °C. The microsphere-like precursor particles showed uniform particle size of around 46 μm, and their surfaces were rough but non-porous, as shown in Fig. 1(b) and 1(d).

When mixing $MgCl_2 \cdot 6H_2O$ with Na_2CO_3 solution at low temperature, for example at 30 °C as practiced in this study, pillar-like precursors were formed immediately. It was found that longer isothermal treatment at low temperature did not change the morphology of precipitated pillar-like precursors. In contrast, the reaction temperature was an important variable to modify the morphology of precursors. Fig. 2 shows SEM images of samples treated at 80 °C after different time intervals. During the hydrothermal treatment, the pillar-like structures changed to microsphere-like structures as reaction time increased. Microsphere-like precursors can be observed in Fig. 2(c), which corresponds to a reaction time of 120 min. After about 160 min, all pillar-like precursors were completely transformed into the microspheres-like precursors.

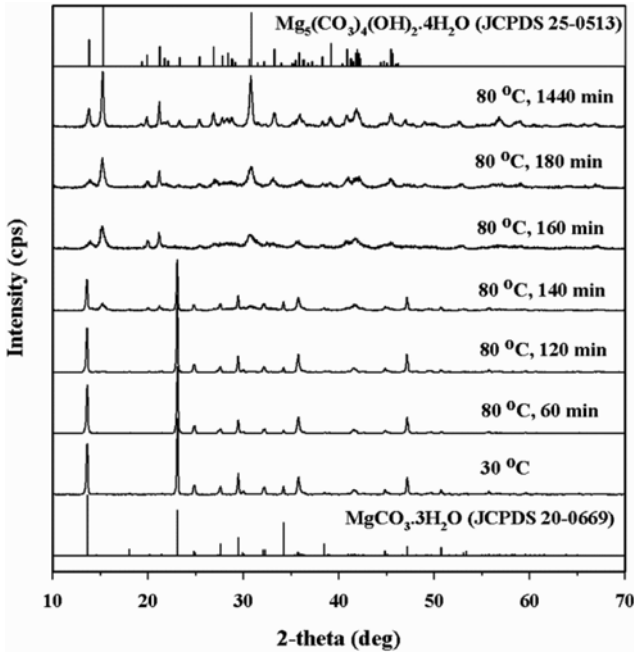

Fig. 3. XRD patterns of pillar-like precursor formed at 30 °C and samples collected after being held at 80 °C for different amounts of time.

Morphology transition from pillar-like precursor to microsphere-like one was explained by considering the change in crystalline structure of precursor [31]. Fig. 3 represents the XRD patterns of samples collected at different time intervals during the hydrothermal treatment at 80 °C, showing the systematic transformation of the chemical structure. Clearly, the pillar and microsphere-like pre-

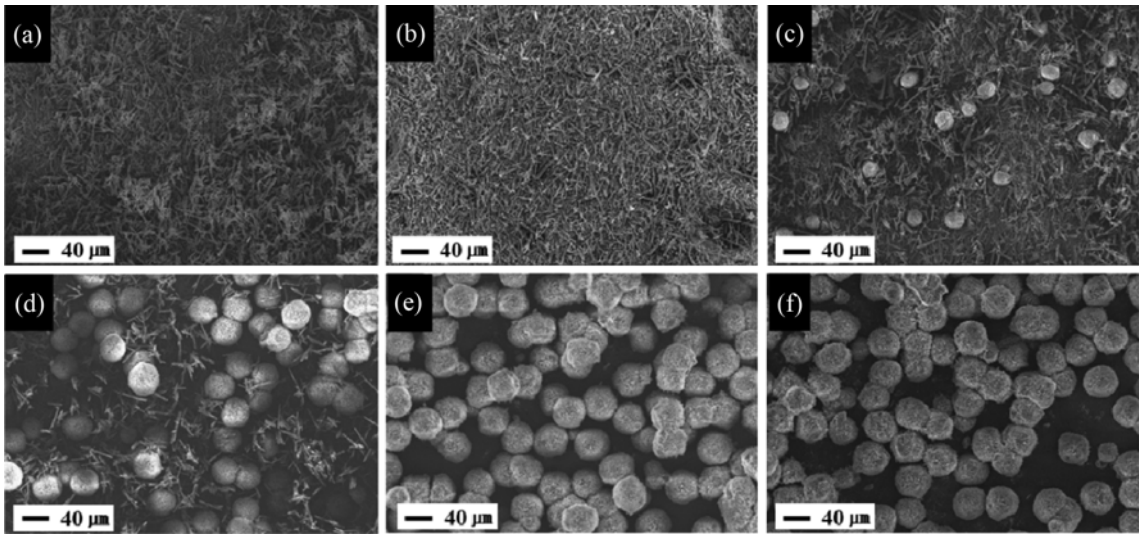

Fig. 2. SEM images of samples collected after isothermal treatment at 80 °C for different amounts of time: (a) 0, (b) 60, (c) 120, (d) 140, (e) 160, and (f) 180 min.

cursors have different crystalline structures. Samples prepared at 30 °C and collected at the earlier state in hydrothermal treatment at 80 °C show the typical XRD pattern of $MgCO_3 \cdot 3H_2O$. XRD patterns related to $Mg_5(CO_3)_4(OH)_2 \cdot 4H_2O$ can be observed after 140 min, and these peaks become more intense as reaction time increases. After approximately 160 min, XRD patterns related to $MgCO_3 \cdot 3H_2O$ have almost disappeared. These results give a good indication that the change in the morphology of the precursor at 80 °C shown in Fig. 2 was a result of transformation from $MgCO_3 \cdot 3H_2O$ to $Mg_5(CO_3)_4(OH)_2 \cdot 4H_2O$.

The hydrothermal treatment for synthesis of microsphere-like precursors of MgO has been usually conducted at a higher temperature above the boiling temperature of water under high pressure [27,31]. In this study, we observed that microsphere-like precursors could be synthesized at much lower temperature. It is surely advantageous in many practical aspects such as equipment design and process safety. The morphology of microsphere-like precursors obtained in this study is almost the same as that prepared at the higher temperature reported in literature [31], except the size of precursors. On the other hand, there is a considerable difference in the time required for complete transition from pillar-like to microsphere-like morphology, that is, it took more than 2 h at 80 °C whereas less than 1 h at 120 °C. Therefore, hydrothermal treatment at higher temperatures has an advantage only from a kinetical point of view. The minimum temperature for the hydrothermal treatment aiming preparation of microsphere-like $Mg_5(CO_3)_4(OH)_2 \cdot 4H_2O$ from $MgCO_3 \cdot 3H_2O$ can be speculated by considering solubility and stability of $MgCO_3 \cdot 3H_2O$ in aqueous solution. It was reported that $MgCO_3 \cdot 3H_2O$ is stable in pure water up to 50 °C and the presence of salts such as NaCl, NH_4Cl, KCl or $MgCl_2$ affects the stability of $MgCO_3 \cdot 3H_2O$ [34].

As a next step to prepare efficient adsorbents for fluoride removal, the as-prepared pillar and microsphere-like precursors were calcined in air at 500 °C for 6 h. Fig. 4 shows the XRD patterns of the calcined materials. Five significant diffraction peaks were observed at 2θ=36.8, 42.8, 62.2, 74.6, and 78.5°, corresponding to (111), (200), (220), (311) and (222) planes of MgO. Meanwhile, the average crystallite size (D=9.4 nm) of microsphere-like MgO determined by Scherrer's Equation ($D=0.89\lambda/\beta\cos\theta$) using full width at half-maximum (β) of the XRD spectrum at 2θ=42.8° was slightly smaller than that of pillar-like MgO (D=10.4 nm).

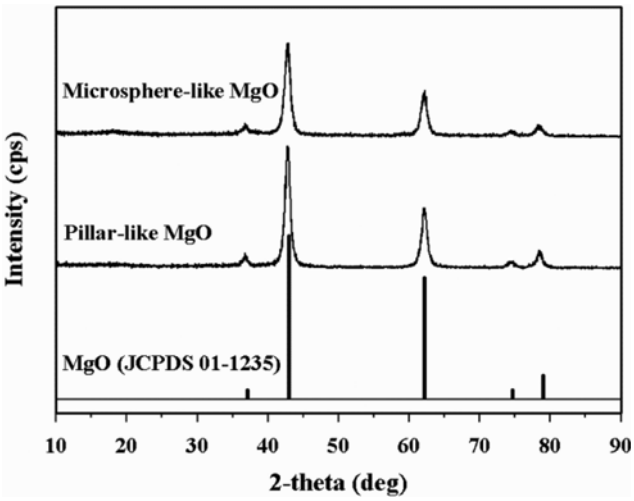

Fig. 4. XRD patterns of MgO prepared from the calcination of pillar and microsphere-like precursors at 500 °C for 6 h.

Fig. 5 shows SEM and TEM images of the pillar and microsphere-like MgO prepared by calcination of precursors. After the calcination process, the surface morphology of the pillar-like MgO

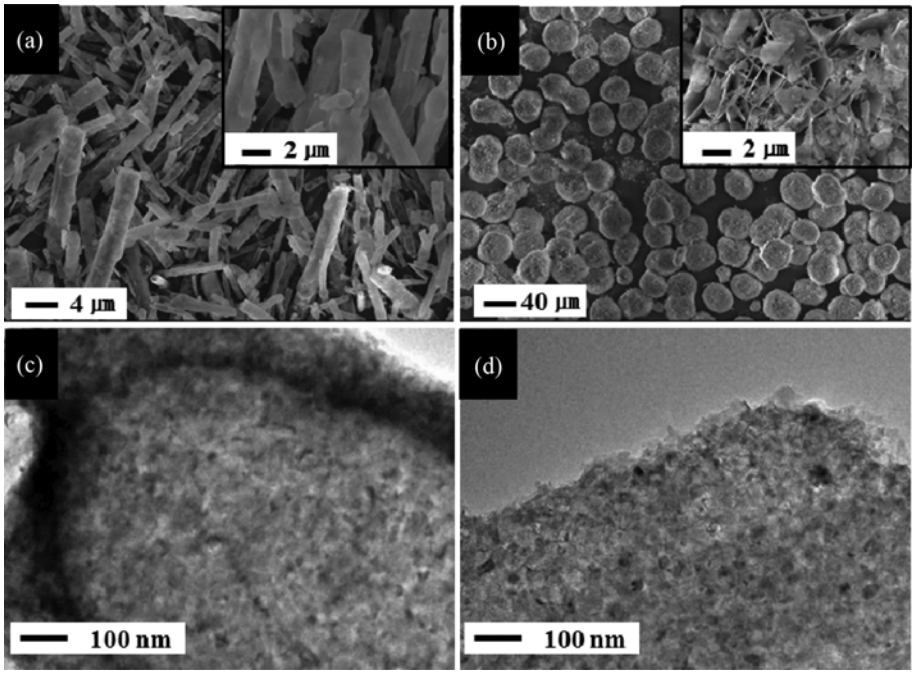

Fig. 5. SEM and TEM images of pillar (a), (c) and microsphere-like MgO (b), (d).

became rough, and a porous structure can be observed in the TEM image (Fig. 5(c)). In the case of microsphere-like MgO, the size of the microspheres and plicate flakes decreased in comparison with the corresponding precursor. As shown in Fig. 5(d), the flakes clearly exhibit a porous structure.

The changes in the specific surface area of the pillar and microsphere-like samples before and after calcination were measured using BET gas sorption analysis as shown in Fig. 6. The pillar-like precursor had a specific surface area of 7.08 m^2/g, while the microsphere-like precursor had a specific surface area of 31.36 m^2/g (Fig. 6(a)). As expected, the thin plicate flakes of the latter sample likely contributed to the high surface area. After calcination, the pillar-like MgO had a specific surface area of 99.44 m^2/g, which is 14 times greater than that of the corresponding precursor. In the case of the microsphere-like MgO, the sample had a specific surface area of 120.74 m^2/g. The pillar-like MgO showed a set of nanopores with a pore size of 6.26 nm, as can be seen in the pore size analysis of the sample in Fig. 6(b). Compared to the pillar-like MgO, the microsphere-like MgO showed two sets of nanopores with sizes of 3.34 and 5.12 nm. In addition, larger pores associated with packing voids are observed. The mesoporous structures of the samples contributed to the increase in the specific surface areas. High surface area MgO derived from calcination is a promising candidate for various applications, including superconductors, paint, catalysis, and toxic waste treatment. In this study, adsorption of fluoride from aqueous solutions was examined.

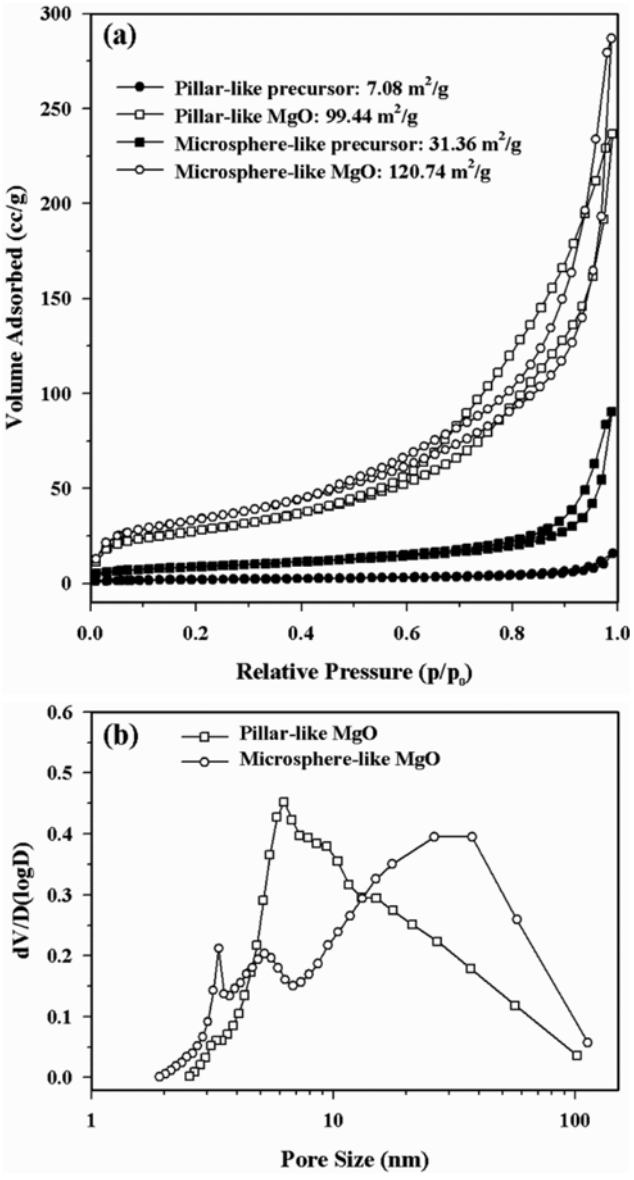

Fig. 6. (a) Nitrogen adsorption-desorption isotherms of as-prepared samples and (b) pore size distributions of pillar and microstructure-like MgO samples.

2. Fluoride Adsorption

The kinetics of fluoride adsorption onto as-prepared samples was studied and the results are shown in Fig. 7(a). MgO samples showed higher fluoride removal efficiencies than their precursors with different chemical structures and specific surface areas. It took about 50 min to reach the adsorption equilibrium in the cases of MgO. It can be found that the fluoride adsorption capacities as

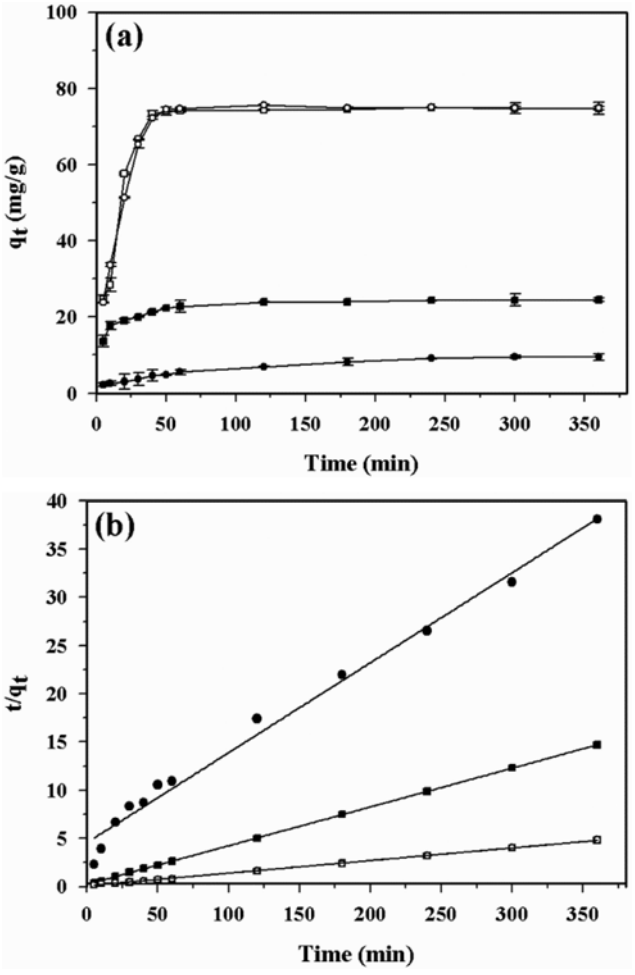

Fig. 7. (a) Kinetics and (b) pseudo-second-order plots of fluoride adsorption by samples before and after calcination: (■) Pillar-like precursor, (●) microsphere-like precursor, (□) pillar-like MgO, and (○) microsphere-like MgO (C_0=100 mg/L, adsorbent dosage=1.0 g/L).

Table 1. Kinetics parameters for fluoride adsorption

Equations[a]	Pseudo-first-order equation $\ln(q_e - q_t) = \ln q_e - k_1 t$				Pseudo-second-order equation $\frac{t}{q_t} = \frac{1}{k_2 q_e^2} + \frac{t}{q_e}$		
	$q_{e,exp}$	k_1	$q_{e,cal}$	R^2	k_2	$q_{e,cal}$	R^2
Pillar-like precursor	24.42	0.0198	7.75	0.9693	7.16×10^{-3}	24.87	0.9999
Microsphere-like precursor	9.33	0.0127	8.33	0.9638	1.90×10^{-3}	10.72	0.9868
Pillar-like MgO	74.72	0.0166	9.31	0.6866	2.13×10^{-3}	76.34	0.9986
Microsphere-like MgO	74.85	0.1093	144.88	0.9600	2.16×10^{-3}	76.92	0.9989

[a]$q_{e,exp}$ and $q_{e,cal}$ are the experimental adsorption capacity and the calculated adsorption capacity (mg/g), respectively. k_1 is the rate constant of pseudo-first-order equation (1/min). k_2 is the rate constant of pseudo-second-order equation (g/(mg·min)). R^2 is the coefficient of regression

well as adsorption kinetics of the pillar and microsphere-like MgO were almost the same. To describe the kinetics of the fluoride adsorption in a better manner, adsorption data were fitted using pseudo-first-order and pseudo-second-order-equations. The kinetic parameters obtained from models are summarized in Table 1. According to the results, kinetic data fit relatively well with the pseudo-second-order equation, which is evident from high R^2. The kinetic plots generated by pseudo-second-order equation are given in Fig. 7(b).

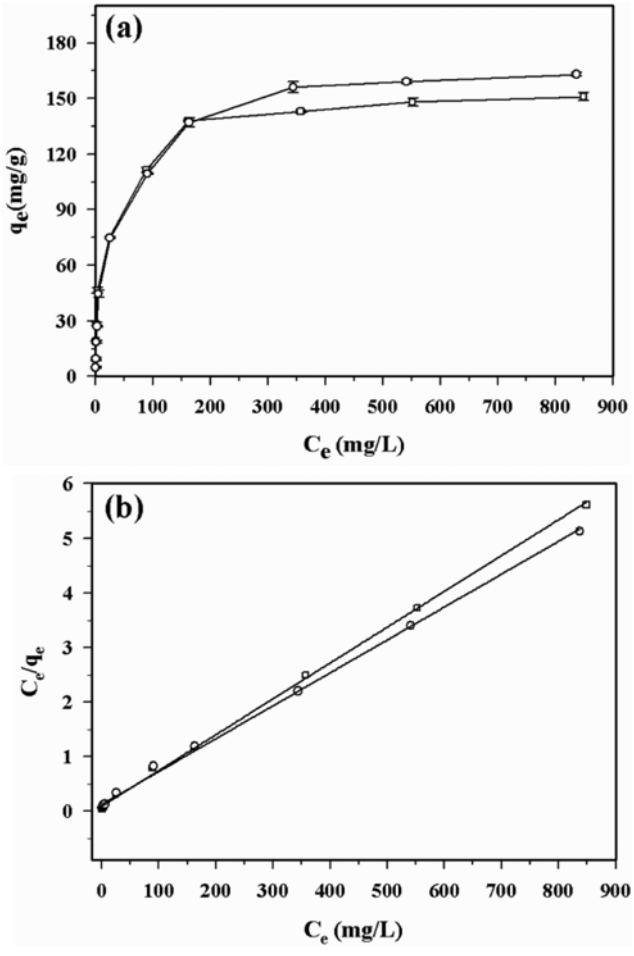

Fig. 8. (a) Adsorption isotherm and (b) Langmuir plots for fluoride adsorption by (□) pillar and (○) microsphere-like MgO (adsorbent dosage=1.0 g/L).

We also investigated the fluoride adsorption equilibria in the range of fluoride concentrations from 5 to 1,000 mg/L. As shown in Fig. 8, the adsorption capacities of the MgO samples exhibited a similar value when the equilibrium fluoride concentration was less than 300 mg/L. Above that concentration, a noticeable difference of adsorption capacities between two samples was observed. The microsphere-like MgO exhibited an improved adsorption capacity compared to pillar-like MgO because of the larger specific surface area. The adsorption equilibrium was analyzed using various isotherm models, including the Langmuir, Freundlich, and Dubinin-Radushkevich isotherms [35,36]. In addition, the chi-square (χ^2) was calculated for all adsorption isotherms using the following equation:

$$\chi^2 = \sum \frac{(q_{e,cal} - q_{e,exp})^2}{q_{e,exp}} \quad (3)$$

where $q_{e,cal}$ is the calculated capacity (mg/g) obtained from the adsorption model and $q_{e,exp}$ is the equilibrium capacity (mg/g) from the experimental data.

The calculated isotherm parameters from the three models are given in Table 2. According to the results, the fluoride adsorption of the pillar and microsphere-like MgO fitted relatively well with the Langmuir model, which is evident from high R^2 and low χ^2. In addition, the maximum fluoride adsorption capacity of pillar and microsphere-like MgO was 151.51 and 166.66 mg/g, respectively.

Fig. 9 shows SEM images of the samples after fluoride adsorption. As shown in Fig. 9(a), assembled plicate flakes were observed on the surface of the pillar-like MgO. On the other hand, the plicate flakes of the microsphere-like MgO were significantly smaller than those observed before fluoride adsorption. A comparison of the plicate flakes of the two samples reveals that the flakes formed on the pillar-like MgO were both smaller and denser. Considering this surface change in the pillar-like MgO after fluoride adsorption, we assume that the adsorption capacity of the pillar-like MgO can be attributed to the occurrence of plicate flakes.

MgO adsorbents remove fluoride ions from aqueous solutions by a surface ion-exchange process that can be expressed by Eqs. (4) and (5) [8,27,37].

$$MgO + H_2O \rightarrow Mg(OH)_2 \quad (4)$$

Table 2. Adsorption isotherm parameters for fluoride adsorption by pillar and microsphere-like MgO with various isotherm models

Isotherm models[a]	Langmuir $q_e=\frac{q_m k_L C_e}{1+k_L C_e}$				Freundlich $q_e=k_F \cdot C_e^{1/n}$				Dubinin-Radushkevich $q_e=q_m \exp(-k_D \cdot \varepsilon^2)$			
	k_L	q_m	R^2	χ^2	n	k_F	R^2	χ^2	k_D	q_m	R^2	χ^2
Pillar-like MgO	0.071	151.51	0.9988	51.00	2.644	17.069	0.8987	60.34	0.0008	113.79	0.9417	59.55
Microsphere-like MgO	0.047	166.66	0.9980	28.26	2.383	14.113	0.9397	55.19	0.0009	102.52	0.8488	145.86

[a]k_L is the Langmuir constant related to the adsorption energy (L/mg) and q_m is the maximum fluoride adsorption capacity of the absorbent (mg/g). k_F is the Freundlich constant related to the relative adsorption capacity of the absorbent (mg/g), and n is the adsorption intensity. k_D is the Dubinin-Radushkevich isotherm constant related to the adsorption energy (mol^2/kJ^2) and ε is the Dubinin-Radushkevich isotherm constant defined as $\varepsilon=RT\ln(1+1/C_e)$, where R is a gas constant (8.314 J/mol K) and T is absolute temperature (K)

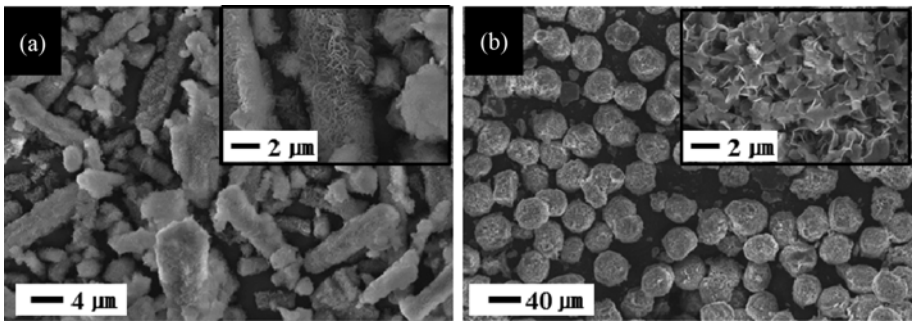

Fig. 9. SEM images of (a) pillar and (b) microsphere-like MgO after fluoride adsorption.

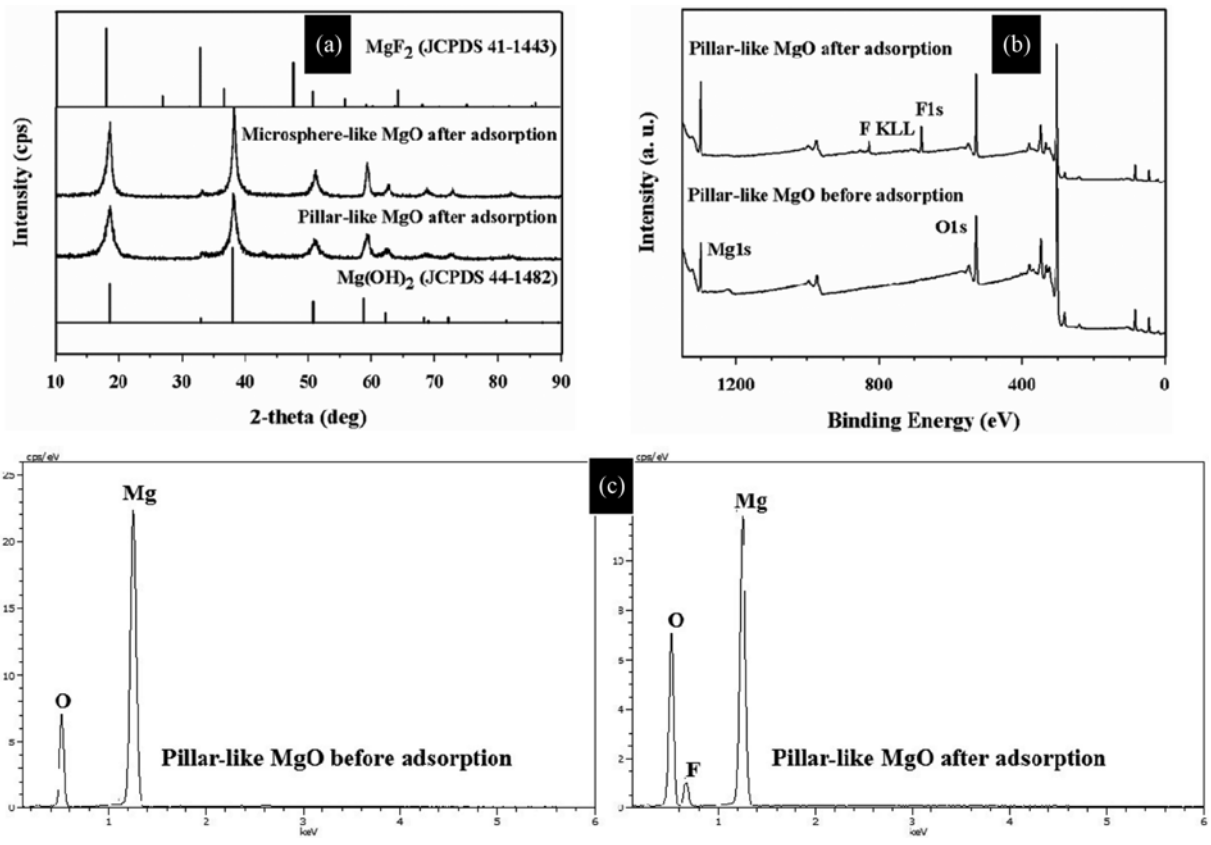

Fig. 10. (a) XRD patterns of pillar and microsphere-like MgO after fluoride adsorption, (b) XPS survey spectra and (c) EDS spectra of pillar-like MgO before and after fluoride adsorption.

$$Mg(OH)_2 + xF^- \rightarrow Mg(OH)_{2-x}F_x + xOH^- \quad (5)$$

To confirm the presence of adsorbed fluorine, samples before and after fluoride adsorption were characterized by XRD, XPS, and EDS. Fig. 10(a) shows the XRD patterns of the MgO samples before and after adsorption of fluoride. It is obvious that the diffraction peaks relevant to MgF_2 were not seen, and only the peaks associated with $Mg(OH)_2$ were detected. On the other hand, the existence of fluorine in the sample after adsorption could be confirmed by EDS analysis (Fig. 10(b)). Furthermore, the XPS survey spectrum shows a peak located at 684 eV after fluoride adsorption (Fig. 10(c)). This new peak can be assigned to the F1s spectrum. The results demonstrate that fluoride removal occurred via substitution of hydroxyl groups in the $Mg(OH)_2$ lattice by fluoride, as shown above in Eqs. (4) and (5).

The effect of pH on the fluoride adsorption onto the MgO samples is shown in Fig. 11(a). Fluoride removal efficiencies gradually decreased with increasing pH from 3.0 to 9.0. Significant reduction in fluoride removal efficiencies was observed at higher pH. It is well known that positive or negative surface sites are developed on the surface of oxides or hydroxides in aqueous suspensions due to the protonation-deprotonation behavior, which can be characterized in terms of the point of zero charge (pzc). In the case of MgO, pzc values ranged from 10 to 12 depending on the measurement methods [38-42]. Therefore, the positive surface charges of MgO decreases as the pH increases and negative surface charges are developed at higher pH above the pzc. Although ion exchange between hydroxide and fluoride is the main mechanism of fluoride removal by MgO as mentioned previously, this result indicates that the ionic interaction between fluoride ions and surface charge of MgO is also important in the adsorption process.

Fig. 11 also shows the effect of other anions on the fluoride removal. In this study, we considered the effect of HCO_3^-, CO_3^{2-}, and PO_4^{2-} on the fluoride adsorption. The fluoride removal efficiencies of the MgO samples were slightly decreased as the concentration of CO_3^{2-} or HCO_3^- increased. The presence of PO_4^{3-} produced a negative effect on fluoride adsorption. The removal efficiency of the pillar and microsphere-like MgO samples decreased abruptly in the presence of 1 mM PO_4^{3-}. Furthermore, when the concentration of PO_4^{3-} was increased to 10 mM, both samples hardly adsorbed any fluoride.

Finally, the regeneration and recyclability of MgO samples were examined, and the results are shown in Fig. 12. Experimental conditions for fluoride adsorption were identical to those described in the adsorption kinetics experiments. Five consecutive adsorption-regeneration cycles were carried out. The removal efficiency of pillar-like MgO at the initial fluorine concentration of 100 mg/L decreased from 75.0% to 40.0% after the first cycle. After five cycles, the removal rate decreased to 26.1%. The removal efficiency of microsphere-like MgO showed a similar value and trend to the results with pillar-like MgO. Deteriorated adsorption performance of regenerated adsorbents is commonly reported in the case of MgO [23,27]. Significant reduction of fluoride removal efficiencies observed in regenerated MgO adsorbents is also an evidence

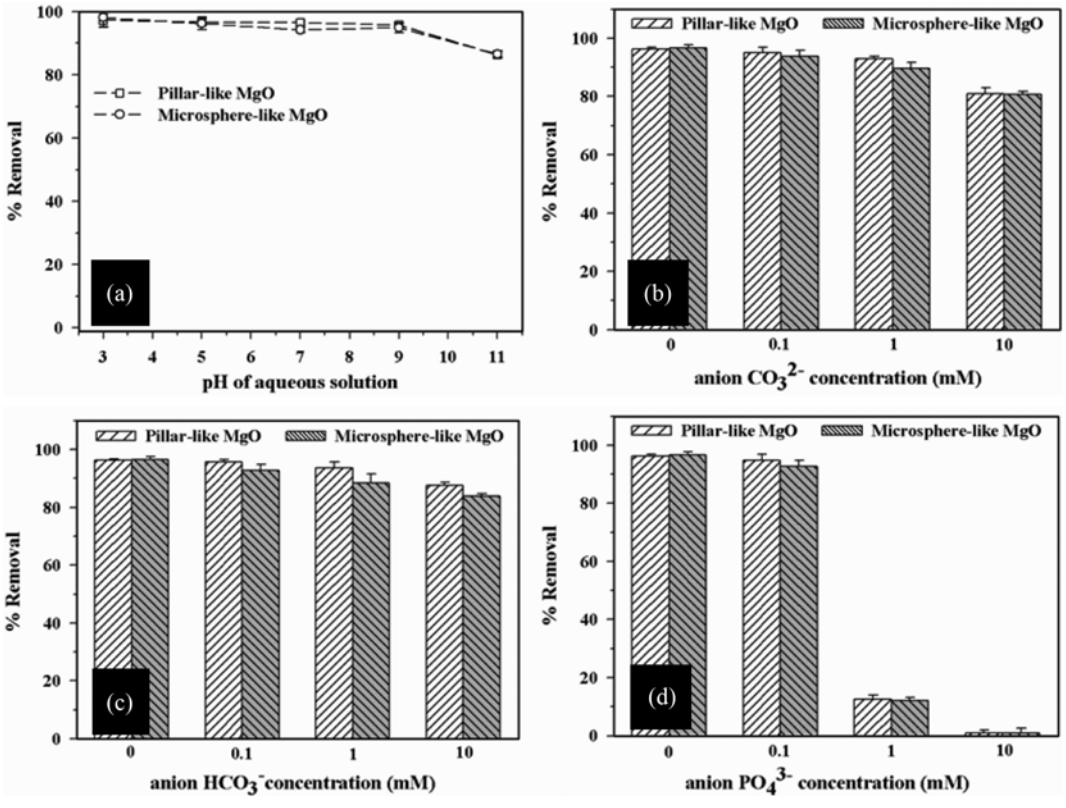

Fig. 11. Effect of pH (a) and the presence of other anions (b), (c), and (d) on fluoride removal efficiency of pillar and microsphere-like MgO (C_0=10 mg/L, adsorbent dosage=1.0 g/L).

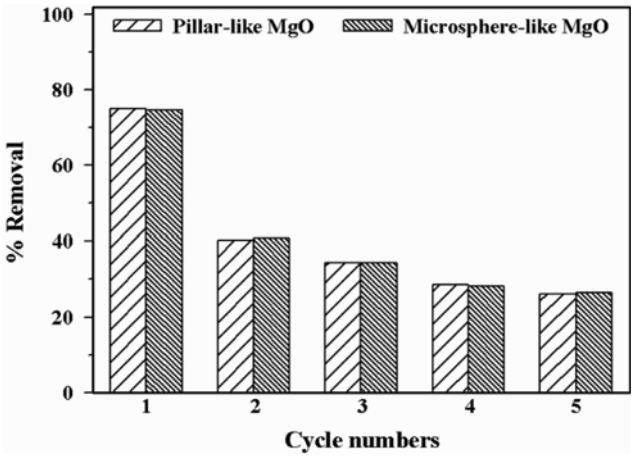

Fig. 12. The fluoride removal efficiency of regenerated pillar and microsphere-like MgO adsorbents (C_0=100 mg/L, adsorbent dosage=1.0 g/L).

indicating the mechanism of fluoride removal is destructive chemisorption resulted from substitution of hydroxyl groups by fluoride ions on the MgO surface.

CONCLUSIONS

Pillar and microsphere-like MgO particles were obtained by calcination of precursors derived from $MgCl_2 \cdot 6H_2O$ at 30 °C and 80 °C, respectively. The pillar-like MgO was approximately 20 μm in length and 2 μm in diameter. In contrast, the microsphere-like MgO consisted of an assembly of flakes and had a diameter of about 30 μm. The specific surface areas of pillar and microsphere-like MgO were 99.44 and 120.74 m^2/g. These MgO samples were applied to the fluoride adsorption process. The adsorption isotherm could be accurately described by the Langmuir model for both samples. The adsorption capacities of pillar and microsphere-like MgO adsorbents were 151.51 and 166.66 mg/g, respectively. Solution pH had little effect on fluoride adsorption below pH 9.0. The study on the effects of various other anions indicated that most of the anions had little effect on fluoride removal efficiencies of both MgO samples, with the exception of phosphate.

ACKNOWLEDGEMENT

This project is supported by the R&D Center for reduction of Non-CO_2 Greenhouse gases (2013001690007) funded by Korea Ministry of Environment as Global Top Environment R&D Program.

NOMENCLATURE

C_0 : initial fluoride concentration [mg/L]
C_e : equilibrium fluoride concentration [mg/L]
k_1 : pseudo-first-order rate constant of adsorption [1/min]
k_2 : pseudo-second-order rate constant of adsorption [g/(mg·min)]
k_D : Dubinin-Radushkevich isotherm constant [mol^2/kJ^2]
k_F : Freundlich isotherm constant [mg/g]
k_L : Langmuir isotherm constant [L/mg]
q_e : adsorption capacity at equilibrium [mg/g]
q_t : adsorption capacity at time [mg/g]
$q_{e,exp}$: experimental adsorption capacity [mg/g]
$q_{e,cal}$: calculated adsorption capacity [mg/g]
q_m : maximum adsorption capacity [mg/g]
m : amount of adsorbent [g]
n : Freundlich adsorption intensity
R^2 : coefficient of regression
V : volume of the fluoride solution [L]
ε : Dubinin-Radushkevich isotherm constant
χ^2 : chi-squared distribution

REFERENCES

1. T. Tsutsui, N. Suzuki, M. Ohmori and H. Maizumi, *Mutat. Res.*, **139**, 193 (1984).
2. A. G. Wang, T. Xia, Q. L. Chu, M. Zhang, F. Liu, X. M. Chen and K. D. Yang, *Biomed. Environ. Sci.*, **17**, 217 (2004).
3. R. P. Liu, W. X. Gong, H. C. Lan, Y. P. Gao, H. J. Liu and J. H. Qu, *Chem. Eng. J.*, **175**, 144 (2011).
4. J. De Zuane, Handbook of Drinking Water Quality, 2nd Ed., Wiley, New York (1996).
5. A. Bhatnagar, E. Kumar and M. Sillanpaa, *Chem. Eng. J.*, **171**, 811 (2011).
6. S. Jagtap, M. K. Yenkie, N. Labhsetwar and S. Rayalus, *Chem. Rev.*, **112**, 2454 (2012).
7. P. Loganathan, S. Vigneswaran, J. Kandasamy and R. Naidu, *J. Hazard. Mater.*, **248**, 1 (2013).
8. K. Zhang, S. Wu, X. Wang, J. He, B. Sun, Y. Jia, T. Luo, F. Meng, Z. Jin, D. Lin, W. Shen, L. Kong and J. Liu, *J. Colloid Interface Sci.*, **446**, 194 (2015).
9. S. V. Mohan, S. V. Ramanaiah, B. Rajkumar and P. N. Sarma, *Bioresour. Technol.*, **98**, 1006 (2006).
10. X. Fan, D. J. Parker and M. D. Smith, *Water Res.*, **37**, 4929 (2003).
11. E. Kumar, A. Bhatnagar, U. Kumar and M. Sillanpaa, *J. Hazard. Mater.*, **186**, 1042 (2011).
12. K. Babaeivelni and A. P. Khodadoust, *J. Colloid Interface Sci.*, **394**, 419 (2013).
13. L. Lv, J. He, M. Wei, D. G. Evans and X. Duan, *J. Hazard. Mater.*, **133**, 119 (2006).
14. Y. Deng, C. Deng, D. Qi, Liu, J. Liu, X. Zhang and D. Zhao, *Adv. Mater.*, **21**, 1377 (2009).
15. D. Y. Zhang, H. M. Luo, L. W. Zheng, K. J. Wang, H. X. Li, Y. Wang and H. X. Feng, *J. Hazard. Mater.*, **241**, 418 (2012).
16. C. T. Yavuz, J. T. Mayo, W. W. Yu, A. Prakash, J. C. Falkner, S. Yean, L. L. Cong, H. J. Shipley, A. Kan, M. Tomson, D. Natelson and V. L. Colvin, *Science*, **314**, 964 (2006).
17. J. S. Hu, L. S. Zhong, W. G. Song and L. J. Wan, *Adv. Mater.*, **20**, 2977 (2008).
18. M. Hua, S. J. Zhang, B. C. Pan, W. M. Zhang, L. Lv and Q. X. Zhang, *J. Hazard. Mater.*, **211**, 317 (2012).
19. B. Wang, H. B. Wu, L. Yu, R. Xu, T. T. Lim and X. W. Lou, *Adv. Mater.*, **24**, 1111 (2012).
20. I. Emmanuelawati, J. Yang, J. Zhang, H. W. Zhang, L. Zhou and

C. Z. Yu, *Nanoscale*, **5**, 6173 (2013).
21. J. Yang, H. W. Zhang, M. H. Yu, I. Emmanuelawati, J. Zou, Z. G. Yuan and C. Z. Yu, *Adv. Funct. Mater.*, **24**, 1354 (2014).
22. B. Nagappa and G. T. Chandrappa, *Micropor. Mesopor. Mater.*, **106**, 212 (2007).
23. K. Sasaki, N. Fukumoto, S. Moriyama, Q. Yu and T. Hirajima, *Sep. Purif. Technol.*, **98**, 24 (2012).
24. V. Gangaiah, A. Siddaramanna and G. T. Chandrappa, *Mater. Res. Exp.*, **1**, 045004 (2014).
25. S. M. Maliyekkal, A. K. R. Antony and T. Pradeep, *Sci. Total Environ.*, **408**, 2273 (2010).
26. R. R. Devi, I. M. Umlong, P. K. Raul, B. Das, S. Banerjee and L. Singh, *J. Exp. Nanosci.*, **9**, 512 (2014).
27. L. X. Li, D. Xu, S. Q. Li, W. C. Liu and Y. Jia, *New J. Chem.*, **38**, 5445 (2014).
28. T. Zhang, H. Yu, Y. Zhou, J. Rong, Z. Mei and F. Qiu, *Korean J. Chem. Eng.*, **33**, 720 (2016).
29. S. C. Lee, S. H. Cha, Y. M. Kwon, M. G. Park, B. W. Hwang, Y. K. Park, H. M. Seo and J. C. Kim, *Korean J. Chem. Eng.*, **33**, 3448 (2016).
30. S. Sadjadi, V. Farzaneh, S. Shrivani and M. Ghashghaee, *Korean J. Chem. Eng.*, **34**, 692 (2017).
31. Y. Qu, W. Zhou, Z. Y. Ren, K. Pan, C. G. Tian, Y. Liu, S. S. Feng, Y. Z. Dong and H. G. Fu, *Eur. J. Inorg. Chem.*, **2012**, 954 (2012).
32. J. B. Zhou, S. L. Yang and J. G. Yu, *Colloids Surf., A: Physicochem. Eng. Aspects*, **379**, 102 (2011).
33. S. Purwajanti, K. Zhou, Y. A. Nor, J. Zhang, H. Zhang, X. Huang and C. Yu, *ACS Appl. Mater. Interfaces*, **7**, 21278 (2015).
34. M. Dong, W. Cheng, Z. Li and G. P. Demopoulos, *J. Chem. Eng. Data*, **53**, 2586 (2008).
35. K. Y. Foo and B. H. Hameed, *Chem. Eng. J.*, **156**, 2 (2010).
36. R. Saadi, Z. Saadi, R. Fazaeli and N. E. Fard, *Korean J. Chem. Eng.*, **32**, 787 (2015).
37. S. M. Maliyekkal, S. Shukla, L. Philip and I. M. Nambi, *Chem. Eng. J.*, **140**, 183 (2008).
38. S. Zalac and N. Kallay, *J. Colloid Interface Sci.*, **149**, 233 (1992).
39. S. Russo and C. Noguera, *Surf. Sci.*, **262**, 245 (1992).
40. K. Bourikas, J. Vakros, C. Kordulis and A. Lycourghiotis, *J. Phys. Chem.*, B **107**, 9441 (2003).
41. M. Kosmulski, *J. Colloid Interface Sci.*, **275**, 214 (2004).
42. K. Bourikas, C. Kordulis and A. Lycourghiotis, *Environ. Sci. Technol.*, **39**, 4100 (2005).